



Cite this: DOI: 10.1039/d0nj02913k

# A new chloro-substituted dicyanoisophorone-based near-infrared fluorophore with a larger Stokes shift and its application for detecting cysteine in cells and *in vivo*†

 Yu Wang,<sup>‡a</sup> Wenda Zhang,<sup>‡\*</sup> Ting Ma,<sup>‡c</sup> Duolu Li,<sup>b</sup> Yubing Zhou,<sup>b</sup> Xiaojian Zhang<sup>\*bde</sup> and Jianbo Gao<sup>\*a</sup>

Many dicyanoisophorone-based fluorophores with an optical hydroxyl group have been explored to meet different imaging needs along with the rapid and wide development of molecular fluorescence bioimaging in recent years. However, most of them used to need the addition of slight alkaline conditions to dissociate a proton for near-infrared emission and this limits their wider application in complex bio-systems. Aiming to modify the dicyanoisophorone-based fluorophore platform with an optically tunable hydroxyl group for better biocompatibility for molecular bioimaging *in vivo*, we developed a new chloro-substituted dicyanoisophorone-based near-infrared fluorophore (**DCM-COH**) which featured simple preparation (two steps), good optical properties and showed potential application prospects. As a proof-of-concept, **DCM-COH** was applied to design a new probe (**CYS-1**) for detecting cysteine. **CYS-1** ( $\lambda_{\text{ex/em}} = 490/655 \text{ nm}$ ) possessed a large Stokes shift (165 nm), low toxicity, good sensitivity (detection limit of  $\sim 173 \text{ nM}$ ) and selectivity for rapid cysteine detection. More importantly, **CYS-1** successfully served as an indicator for imaging cysteine in cells and *in vivo*. Fluorophore **DCM-COH** may act as a potential platform to be extended as a capable tracking tool in biological chemistry and preclinical applications.

 Received 10th June 2020,  
 Accepted 8th August 2020

DOI: 10.1039/d0nj02913k

[rsc.li/njc](http://rsc.li/njc)

## Introduction

In recent years, molecular fluorescence bio-imaging technology has attracted more and more attention due to its advantages of high temporal and spatial resolution, high sensitivity, strong specificity, simple operation, fast detection response and so on.<sup>1–6</sup> It has been used as a powerful strategy to detect enzyme activity or small biological species in pathophysiological elucidation and disease diagnosis of related diseases.<sup>7–9</sup> However, to trace and visualize related biological species in the complexity

of dynamic life systems is difficult.<sup>1,3</sup> In order to meet the complex imaging needs, a variety of fluorophores have been developed. Among them, the molecular fluorophores with an optically tunable hydroxyl group play an important role in the development of activated fluorescent probes, the hydroxyl group of which was regulated through the protection and deprotection of hydroxyl groups.<sup>10–12</sup> The design rule is shown in Fig. 1. When the characteristic hydroxyl group is protected by a trigger group, the fluorescence of the probe is “turned off” or

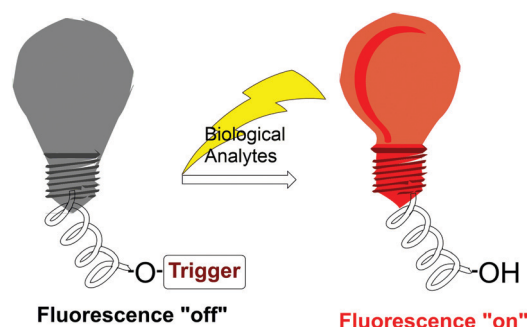


Fig. 1 Design principle of molecular probes for biological analytes through hydroxyl regulation.

<sup>a</sup> Department of Radiology, The First Affiliated Hospital of Zhengzhou University, No. 1, East Jianshe Road, Zhengzhou 450052, Henan, China.  
 E-mail: gaojianbo63@126.com

<sup>b</sup> Department of Pharmacy, The First Affiliated Hospital of Zhengzhou University, No. 1, East Jianshe Road, Zhengzhou 450052, Henan, China.  
 E-mail: zhangwenda16@126.com, zhangxiaojian15@126.com

<sup>c</sup> School of Pharmaceutical Sciences, Zhengzhou University, Zhengzhou 450001, China

<sup>d</sup> Henan Key Laboratory of Precision Clinical Pharmacy, Zhengzhou University, Zhengzhou, China

<sup>e</sup> Henan Engineering Research Center of Clinical Mass Spectrometry for Precision Medicine, Zhengzhou, China

† Electronic supplementary information (ESI) available. See DOI: 10.1039/d0nj02913k

‡ These authors contributed equally.

the semichromatic displacement is displayed due to the weakening of the electron donor capacity. The characteristic hydroxyl trigger group of the fluorophore is cleaved under the action of a special analyst to produce a wide emission fluorescence signal.

So far, many molecular fluorophores with optical hydroxyl groups have been constructed, such as coumarin,<sup>13–16</sup> naphthalimide,<sup>17,18</sup> indanone,<sup>19</sup> rhodol,<sup>12,20</sup> dicyanomethylene-4*H*-pyran (DCM),<sup>21</sup> BODIPY,<sup>10</sup> and HD dye,<sup>22,23</sup> which are widely used due to their photophysical properties (Fig. 2). However, the application of these fluorophores in biological systems is still challenging, due to the short emission wavelength (<600 nm) of coumarin, naphthalimide and rhodol, the short Stokes shift of fluorescein and HD dyes, and the complex preparation of BODIPY. Interestingly, dicyanophosphorone fluorophores exhibit short wavelength emission under physiological conditions, while they exhibit near-infrared red emission in dimethyl sulfoxide or other organic solvents.<sup>11,24–29</sup> Although dicyanophosphorone fluorophores have the advantages of simple synthesis, good water solubility, a large Stokes shift and good biocompatibility, adding more dimethyl sulfoxide or other organic solvents in the detection system will cause enzyme degradation or damage the organisms, and this limits its application in the living system. This encourages us to develop new NIR fluorescent carriers with better biocompatibility for *in vivo* molecular imaging.

In this study, a new near-infrared emission fluorophore **DCM-COH** was developed. It did not need a high proportion of DMSO or other organic solvents, but exhibited long emission wavelength and a large Stokes shift under physiological conditions. In addition, it has excellent chemical and optical properties, such as simple preparation (step synthesis), suitable  $pK_a$  (7.60), deep tissue penetration, near-infrared emission in a physiological environment and so on, which showed a broad application prospect. As a proof of concept, it has been successfully applied

to design a new cysteine detection probe (**CYS-1**). **CYS-1** ( $\lambda_{ex/em}$  = 490/655 nm) has a large Stokes shift (165 nm), low toxicity, high sensitivity (detection limit is about 173 nM), and selectivity for the rapid detection of cysteine. **CYS-1** can also be used as an indicator for cysteine imaging in cells and *in vivo* under low background interference.

## Experimental section

### Materials and general experimental methods

Unless specially stated, all chemicals and solvents were supplied by Sinopharm chemical reagent Co. Ltd. Cysteine was obtained from Sigma-Aldrich Co. Ltd. <sup>1</sup>H NMR spectra were measured using a Bruker spectrometer (500 MHz) and <sup>13</sup>C NMR spectra were measured using a Bruker spectrometer (125 MHz). The fluorescence spectra were recorded on a Spectra Max Paradigm Multi-Mode Detection Platform. *In vivo* imaging was performed using a CRI Maestro small animal *in vivo* imaging system.

### Synthesis

**(*E*)-2-(3-(3-Chloro-4-hydroxystyryl)-5,5-dimethylcyclohex-2-en-1-ylidene)malononitrile (DCM-COH)**. To a solution of compound **1** (1.0 g, 5.37 mmol) and piperidine (0.15 mL) in acetonitrile (40 mL) was added 3-chloro-4-hydroxybenzaldehyde (925 mg, 5.91 mmol), the mixture was further stirred at 80 °C for 6 h. After the reaction, the precipitate was filtered, washed, and recrystallized with ethanol to obtained **DCM-COH** as a red crystal (1.2 g, 68.8%). <sup>1</sup>H NMR (500 MHz, CDCl<sub>3</sub>)  $\delta$  7.51 (s, 1H), 7.35 (d,  $J$  = 7.3 Hz, 1H), 7.04 (d,  $J$  = 8.4 Hz, 1H), 6.93 (d,  $J$  = 16.1 Hz, 1H), 6.85 (d,  $J$  = 16.1 Hz, 1H), 6.82 (s, 1H), 5.75 (s, 1H), 2.60 (s, 2H), 2.44 (s, 2H), 1.08 (s, 6H). <sup>13</sup>C NMR (101 MHz, CDCl<sub>3</sub>)  $\delta$  189.59 (s), 169.20 (s), 156.54 (s), 153.60 (s), 152.58 (s), 135.20 (s), 130.75 (d,  $J$  = 14.8 Hz), 129.66 (s), 128.29 (s), 127.99 (d,  $J$  = 17.8 Hz), 123.45 (s), 121.10 (s), 120.76 (s), 116.79 (d,  $J$  = 14.1 Hz), 113.51 (s), 112.73 (s), 78.66 (s), 42.99 (s), 39.21 (s), 32.05 (s), 28.04 (s). (ESI-MS)  $m/z$  calcd for C<sub>19</sub>H<sub>17</sub>ClN<sub>2</sub>O [M – H]<sup>+</sup>, 323.0957; found 323.0955.

**(*E*)-2-(3-(4-Hydroxystyryl)-5,5-dimethylcyclohex-2-en-1-ylidene)malononitrile (DCI-OH)**. To a solution of compound **1** (1.0 g, 5.37 mmol) and piperidine (0.15 mL) in acetonitrile (40 mL) was added 4-hydroxybenzaldehyde (656 mg, 5.37 mmol), the mixture was further stirred at 80 °C for 6 h. After the reaction, the precipitate was filtered, washed, and recrystallized with ethanol to obtained **DCI-OH** as a red crystal (1.2 g, 69.8%). <sup>1</sup>H NMR (500 MHz, DMSO)  $\delta$  9.97 (s, 1H), 7.55 (d,  $J$  = 8.5 Hz, 2H), 7.21 (d,  $J$  = 8.5 Hz, 2H), 6.83–6.75 (m, 3H), 2.59 (s, 2H), 2.53 (s, 2H), 1.01 (s, 6H). <sup>13</sup>C NMR (101 MHz, CDCl<sub>3</sub>)  $\delta$  191.17 (s), 169.64 (s), 157.51 (s), 154.61 (s), 137.05 (s), 132.57 (s), 129.55 (s), 128.68 (s), 127.12 (s), 122.86 (s), 116.17 (d,  $J$  = 14.7 Hz), 113.84 (s), 113.08 (s), 43.16 (s), 39.36 (s), 32.18 (s), 28.17 (s).

**(*E*)-2-Chloro-4-(2-(3-(dicyanomethylene)-5,5-dimethylcyclohex-1-en-1-yl)vinyl)phenyl acrylate (CYS-1)**. To a solution of **DCM-COH** (0.5 g, 1.54 mmol) and DIPEA (0.58 mL) in dry dichloromethane (10 mL) was added acryloyl chloride (374  $\mu$ L, 4.62 mmol) in 10 mL of dry dichloromethane. Under an air atmosphere, the reaction mixture was stirred at room temperature for 3 h.

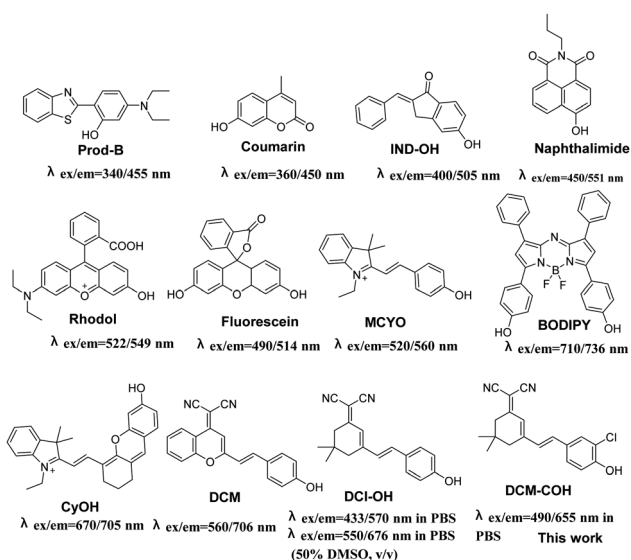


Fig. 2 Structures of reported fluorophores with an optically tunable hydroxyl group.

The resulting organic layer was washed with water and dried over  $\text{Na}_2\text{SO}_4$ . After dichloromethane removal and further purification with silica gel column chromatography (petroleum ether/ethyl acetate), the desired compound **CYS-1** was afforded as a yellow solid (0.51 g, 87.5%).  $^1\text{H}$  NMR (500 MHz, DMSO)  $\delta$  8.00 (d,  $J$  = 1.6 Hz, 1H), 7.71 (dd,  $J$  = 8.4, 1.6 Hz, 1H), 7.52 (d,  $J$  = 16.2 Hz, 1H), 7.42 (d,  $J$  = 8.4 Hz, 1H), 7.28 (d,  $J$  = 16.2 Hz, 1H), 6.93 (s, 1H), 6.61 (d,  $J$  = 17.3 Hz, 1H), 6.47 (dd,  $J$  = 17.2, 10.4 Hz, 1H), 6.24 (d,  $J$  = 10.5 Hz, 1H), 2.63 (s, 2H), 2.53 (s, 2H), 1.02 (s, 6H).  $^{13}\text{C}$  NMR (126 MHz, DMSO)  $\delta$  170.28 (s), 163.13 (s), 155.18 (s), 146.64 (s), 135.89 (s), 134.84 (d,  $J$  = 9.7 Hz), 131.23 (s), 128.57 (s), 127.96 (s), 126.72 (s), 126.52 (s), 124.61 (s), 123.61 (s), 113.70 (s), 112.90 (s), 77.18 (s), 42.24 (s), 38.11 (s), 31.68 (s), 27.44 (s). (ESI-MS)  $m/z$  calcd for  $\text{C}_{22}\text{H}_{19}\text{ClN}_2\text{O}_2$   $[\text{M} - \text{H}]^-$ , 377.1062; found 377.1061.

### General procedure to monitor cysteine *in vitro*

All the spectrum measurements were performed in PBS buffer (10 mM, pH 7.4) at 37 °C. The stock solution of probe **CYS-1** (5 mM) was prepared in DMSO. Various analytes (Gly, Leu,  $\text{KH}_2\text{PO}_4$ ,  $\text{Na}_2\text{SO}_3$ ,  $\text{NaHCO}_3$ ,  $\text{MgSO}_4$ ,  $\text{KAl}(\text{SO}_4)_2$ , KCl, NaAc, KI,  $\text{NaIO}_4$ ,  $\text{CaCl}_2$ , NaCl, GSH, Hcy, and cysteine) were prepared in ultrapure water. The calculated amount of probe in the test solution was prepared at a final concentration of 10  $\mu\text{M}$ . Cysteine and other analytes were also dissolved in test solution with an appropriate concentration. The fluorescence emission spectra were collected ( $\lambda_{\text{ex}}$  = 490 nm,  $\lambda_{\text{em}}$  = 655 nm).

### Activation mechanism

ESI-MS was used to verify the activation mechanism. In detail, **CYS-1** (50  $\mu\text{M}$ ) was incubated with cysteine (50  $\mu\text{M}$ ) for 5 min in PBS solution, then extracted with dichloromethane and concentrated. The concentrated solution was analyzed by ESI-MS.

### Cell culture and cytotoxicity assay

A549 cells were provided by Cell Bank of Shanghai Institute of Biochemistry and Cell Biology, Chinese Academy of Sciences (Shanghai, China), and were grown in DMEM medium supplemented with 10% fetal bovine serum (FBS) at 37 °C in a 5%  $\text{CO}_2$ /95% air incubator. For MTT assays, cells were initially seeded into a 96-well plate at a density of  $6 \times 10^3$  cells per well and incubated for 24 h, and then media were replaced with 200  $\mu\text{L}$  DMEM media with different concentrations (0, 5.0, 10, 20, 30, and 40  $\mu\text{M}$ ) of the probe. After incubation for 24 h 0.02 mL of the MTT (0.5  $\text{mg mL}^{-1}$ ) were added to each well followed by culture for another 4 h. After that, the media were abandoned and the formed formazan was dissolved in 150  $\mu\text{L}$  DMSO in each well. Then, the absorbance values were measured at 570 nm with a reference wavelength of 630 nm using an ELISA reader (Spectra Max Plus 384, Molecular Devices, Sunnyvale, CA) and the cell viability rate was calculated.

### Imaging of cysteine in living cells

Cells were seeded into a 96-well plate and cultured in DMEM medium supplemented with 10% FBS in an atmosphere of 5%  $\text{CO}_2$  at 37 °C. After 24 h, the cells were treated with cysteine (20  $\mu\text{M}$ ), then incubated with 10  $\mu\text{M}$  probe or without probe as control.

A549 cells were treated with **CYS-1** (10  $\mu\text{M}$ ) after incubation with cysteine (20  $\mu\text{M}$ ) and then NEM (1 mM). The images of the cells were taken under a laser confocal microscope.

### *In vivo* imaging of cysteine in living mice

All animal procedures were performed in accordance with the requirements of the Animal Ethics Committee of Zhengzhou University, and the guidelines of the National Institutes of Health. All animal experiments were approved by the Animal Ethics Committee of Zhengzhou University.

For *in vivo* imaging, the mice were divided into two groups. (a) Fluorescence imaging of cysteine in living mouse after intraperitoneal injection of PBS (100  $\mu\text{L}$ ) as blank; (b) fluorescence imaging of cysteine in living mouse after injection of **CYS-1** (200  $\mu\text{M}$ , 50  $\mu\text{L}$ ) followed by treatment with cysteine (200  $\mu\text{M}$ , 50  $\mu\text{L}$ ) for 25 min. Then, the *in vivo* imaging was obtained by using a CRI Maestro small animal *in vivo* imaging system.

## Results and discussion

### Fluorophore structure optimization and performance study

Dicyanoisophorone-based systems with attractive attention have been widely used in bioimaging due to their many advantages including simple synthesis, fine water solubility, a large Stokes shift, excellent biocompatibility and so on. As a dicyanoisophorone-based fluorescent dye, **DCI-OH** has been widely used as a fluorophore to design a variety of fluorescent probes; its excitation and emission wavelengths are 433 nm and 570 nm in PBS solution respectively. Because near-infrared red emissions with higher penetrability can avoid auto-fluorescence interference from indigenous biomolecules compared with the shorter wavelength, many analytical chemists usually force **DCI-OH** to dissociate a proton for NIR emission through the addition of more dimethyl sulphoxide or other organic solvent in detecting systems, which may cause enzyme degeneration to damage organisms in living systems. This encouraged us to modify its structure to develop a new NIR fluorophore with better biocompatibility for molecular bioimaging *in vivo*. The key issue is that the high  $\text{pK}_a$  value of **DCI-OH** leads to its low proton dissociation under physiological conditions and limits its precise bioimaging application *in vivo*.<sup>16,30</sup> Nevertheless, electron-withdrawing substitution at the ortho position of hydroxyl on the fluorophore skeleton can reduce the  $\text{pK}_a$  value of the molecular dye. As expected, new chloro-substituted **DCM-COH** ( $\text{pK}_a$  = 7.60) exhibits a better optical performance under mimetic physiological conditions compared with **DCI-OH** ( $\text{pK}_a$  = 9.02) (Fig. 3). Taken together, **DCM-COH** is more suitable than **DCI-OH** for developing activated *in vivo* bioimaging fluorescent probes.

### Design and synthesis of CYS-1

Cysteine participates in a variety of life activities, and its abnormal change can lead to serious diseases including acquired immunodeficiency syndrome, liver damage and skin damage.<sup>31,32</sup>

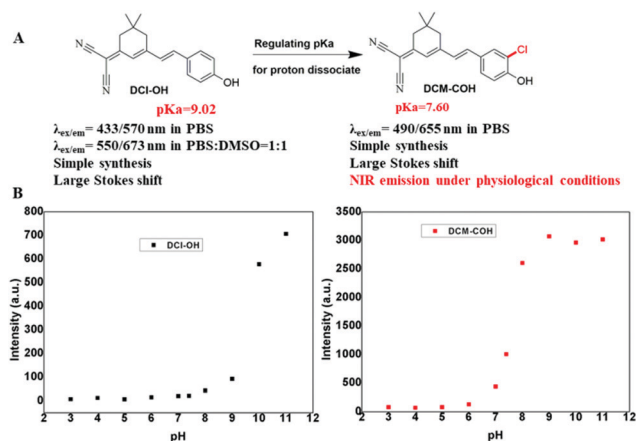


Fig. 3 (A) Structure modification of fluorophore **DCI-OH**. (B) Fluorescence intensity at the maximum emission wavelength of **DCI-OH** and **DCM-COH** vs. pH.

Up to now, many fluorescent probes have been developed for the detection of cysteine, but there is still difficulty in monitoring the *in vivo* cysteine concentration due to their insufficient sensitivity and their short emission wavelengths (Table S1, ESI<sup>†</sup>).<sup>4</sup> Though some NIR fluorescent probes with long excitation wavelengths (> 650 nm) were reported, the relatively short Stokes shift or high proportion of organic solvent in test systems limited further biological applications.<sup>2,33–38</sup> Development of fluorescent probes with a large Stokes shift which can penetrate deeper tissue under physiological conditions for cysteine tracking is still urgent.

As a proof-of-concept, **DCM-COH** was used as an NIR fluorophore for developing a new probe **CYS-1** to detect biomarker cysteine for the first time. Herein, we chose the acryl ester as a selective reaction trigger for cysteine to realize fluorescence “off-on”. After interaction of **CYS-1** with cysteine, the free **DCM-COH** was released, yielding a remarkable fluorescence signal (Fig. 4).

**CYS-1** was synthesized within two steps as shown in Scheme 1, **DCM-COH** or **DCI-OH** was obtained by reaction compound **1** with 3-chloro-4-hydroxybenzaldehyde or 4-hydroxybenzaldehyde. Compound **DCM-COH** in dry dichloromethane was added to acryl chloride to obtain **CYS-1**. The spectra of <sup>1</sup>H NMR and <sup>13</sup>C NMR are shown in Fig. S3–S9 in the ESI.<sup>†</sup>

### Spectral response of **CYS-1** towards cysteine

Firstly, the spectral character of this probe was initially investigated in the buffer solution (PBS, 10 mM, pH = 7.4), which

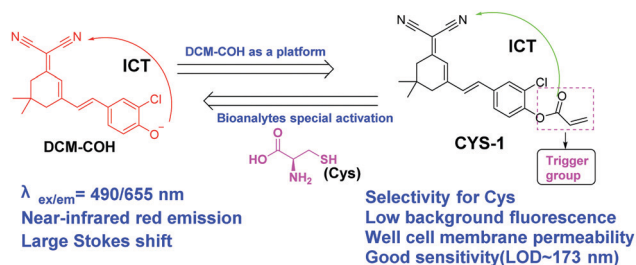
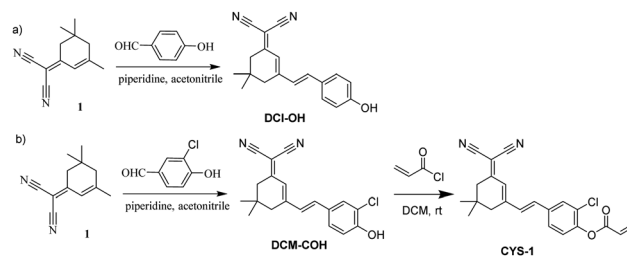


Fig. 4 Design principle of molecular probe **CYS-1** for cysteine detection based on **DCM-COH**.



Scheme 1 Synthesis of **DCM-COH** and probe **CYS-1**.

implied its favorable water solubility. The excitation and emission spectra of **DCM-COH** (10  $\mu$ M) were measured in PBS solution, the maximum excitation and the maximum emission was at 490 nm and 655 nm respectively (Fig. 5A), the NIR emission of **DCM-COH** with an obviously large Stokes shift (165 nm) was suitable for imaging analysis due to the efficiently decreased measurement error caused by the overlapped excitation light and scattered light. The time-dependent fluorescence response of **CYS-1** toward cysteine was tested. As shown in Fig. 5B, the fluorescence intensity at 655 nm increased rapidly with time, and reached the maximum value in approximately 25 min. The significantly increasing maximum fluorescence intensity at 655 nm suggested that the cleavage reaction initiated by cysteine resulted in the release of free **DCM-COH**, indicating that the probe can be used as a fluorescent sensor sensitive to cysteine. Subsequently, with the increase of cysteine concentration, the fluorescence intensity at 655 nm increased gradually. The continuous increase of cysteine resulted in a significant enhancement of fluorescence intensity at 655 nm (Fig. 5C). In the concentration range of 0–150  $\mu$ M, the fluorescence signal intensity has a linear relationship with cysteine ( $R^2 = 0.9993$ , Fig. 5D). The detection limit of the probe ( $3\sigma/\text{slope}$  method) was as low as 173 nM.

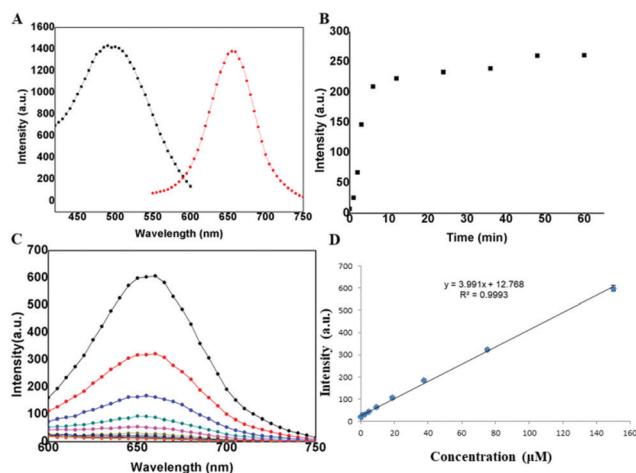


Fig. 5 (A) Excitation and emission spectra of **DCM-COH** (10  $\mu$ M); (B) fluorescence response of 10  $\mu$ M **CYS-1** after incubation with Cys during time in PBS buffer (10 mM, pH 7.4); and (C) fluorescence response of 10  $\mu$ M **CYS-1** after incubation with Cys (0–150  $\mu$ M) in PBS buffer (10 mM, pH 7.4). (D) Linear relationship of fluorescence response of 10  $\mu$ M **CYS-1** with a function of the concentrations of Cys from 0 to 150  $\mu$ M at 655 nm in PBS ( $\lambda_{\text{ex}} = 490$  nm,  $\lambda_{\text{em}} = 655$  nm).

### The detection mechanism of CYS-1 towards cysteine

As aforementioned, the cleavage of acryl ester by the cysteine-reactive reaction could release the electro-donating OH generating DCM-COH. The activation mechanism was verified by electrospray ionization mass spectrometry (ESI-MS). CYS-1 was incubated with cysteine in PBS solution and extracted by dichloromethane and concentrated. The concentrated solution was analyzed by ESI-MS. As shown in Fig. S3–S5 (ESI<sup>†</sup>), the peak at  $m/z$  174.0231  $[M - H]^-$  corresponds to a seven-membered cyclized by-product, the peak at  $m/z$  323.0931  $[M - H]^-$  corresponds to DCM-COH and the peak at  $m/z$  377.1059  $[M - H]^-$  corresponds to CYS-1, indicating that the addition of CYS-1 in the presence of cysteine did produce DCM-COH.

### Selectivity of cysteine

In order to further verify the specificity of the probe for the fluorescence sensing of cysteine, the fluorescence signal changes of the probe to various analytes (including Gly, Leu,  $\text{KH}_2\text{PO}_4$ ,  $\text{Na}_2\text{SO}_3$ ,  $\text{NaHCO}_3$ ,  $\text{MgSO}_4$ ,  $\text{KAl}(\text{SO}_4)_2$ , KCl, NaAC, KI,  $\text{NaIO}_4$ ,  $\text{CaCl}_2$ , NaCl, GSH, Hcy, and cysteine) were recorded. As shown in Fig. 6, the addition of other analytes made the probe exhibit negligible fluorescence response. In conclusion, probe CYS-1 possessed excellent specificity under physiological conditions.

### The detection character of CYS-1 under different pH conditions

In addition, we studied the fluorescence character of the probe at different pH values to study its application in biological imaging (Fig. S1, ESI<sup>†</sup>). No obvious emission changes at 655 nm were observed in the pH range of 6–9, indicating that the probe could remain stable under acidic and alkaline conditions. As expected, in the presence of cysteine, the emission increased distinctly in the pH range from 6–9, especially under the alkaline conditions. The alkaline solution increased the

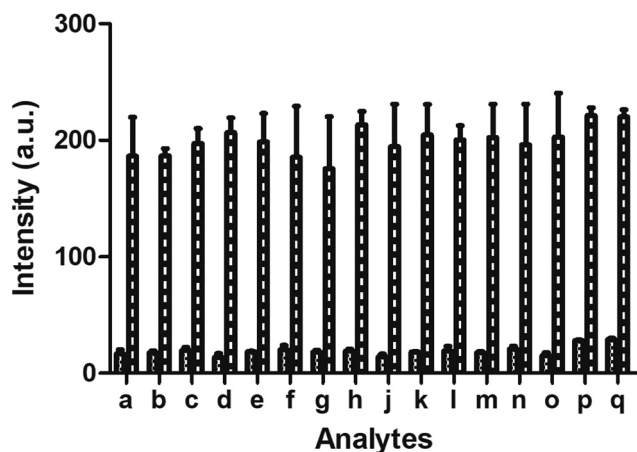


Fig. 6 Fluorescence intensity changes of CYS-1 upon exposure to different types of analytes. Fluorescence intensity at 655 nm of CYS-1 (10  $\mu\text{M}$ ) upon interaction with other analytes (40  $\mu\text{M}$ ) in PBS buffer (10 mM, pH 7.4). Columns a–q: Gly, Leu,  $\text{KH}_2\text{PO}_4$ ,  $\text{Na}_2\text{SO}_3$ ,  $\text{NaHCO}_3$ ,  $\text{MgSO}_4$ ,  $\text{KAl}(\text{SO}_4)_2$ , KCl, NaAC, KI,  $\text{NaIO}_4$ ,  $\text{CaCl}_2$ , NaCl, GSH, Hcy, and cysteine.

ionization of cysteine, promoted the thiolysis reaction to restore the fluorophore. The results showed that the probe has obvious advantage and practical value for the application of bio-imaging in living systems. In order to adapt to the physiological conditions of the cellular system, a pH of 7.4 was selected as the experimental condition.

### The cysteine detection by CYS-1 in bottled water samples

Next, the selectivity of CYS-1 was tested by determining the concentration of Cys in water samples through a recovery test. The fluorescence signal at 655 nm was recorded by adding different Cys to the water sample. As shown in Table 1, CYS-1 determined the concentration of Cys in the water samples, with a good recovery ranging from 98.4% to 101.6%. The results indicated that CYS-1 could be used for the quantitative detection of Cys in water samples.

### Cytotoxicity and cell imaging of CYS-1

The excellent performance of the probe *in vitro* detecting system enabled us to further explore its ability to track cysteine in living cells. Before cellular application, the biocompatibility of the probe on A549 cells was detected by the MTT method. After incubation with a high concentration of 40  $\mu\text{M}$  CYS-1 for 24 h, the survival rate of A549 cells was close to 90%, indicating that the cytotoxicity of the probe on cells was very small (Fig. S2, ESI<sup>†</sup>). We further used the probe to evaluate the intracellular cysteine change in A549 cells. The results in Fig. 7 show that when the probe (10  $\mu\text{M}$ ) was added, a fluorescence signal can be observed indicating that A549 tumor cells contain a certain amount of cysteine. When the cells were pretreated with cysteine (20  $\mu\text{M}$ ) and incubated with the probe (10  $\mu\text{M}$ ), an obvious near-infrared fluorescence signal of living cells was observed, which indicated that the probe had good cell permeability and potential to detect cysteine in living cancer cells.

### *In vivo* imaging of CYS-1 towards cysteine

For accurate disease diagnostics, *in vivo* imaging is a powerful tool particularly for suspicious lesions with high spatio-temporal precision. We examined the applicability of the probe in the *in vivo* detection of the endogenous cysteine. Mice were divided into two groups. In the first group, the mice were injected subcutaneously with PBS (100  $\mu\text{L}$ ) for 25 min as a control. In the second group, the mice were subcutaneously injected with CYS-1 (200  $\mu\text{M}$ , 50  $\mu\text{L}$ ) followed by injection with cysteine (200  $\mu\text{M}$ , 50  $\mu\text{L}$ ) for 25 min. The *in vivo* imaging was captured on a CRI Maestro small animal *in vivo* imaging system. As shown in Fig. 8, almost no fluorescence was observed in the first group. However, a significant NIR fluorescence enhancement

Table 1 Results of the recovery test for applicability evaluation in bottled purified water

Sample no.	Cys spiked ( $\mu\text{M}$ )	Recovered ( $\mu\text{M}$ )	Recovery (%)
1	50	$49.0 \pm 0.75$	98.4
2	100	$100.2 \pm 3.7$	101.6

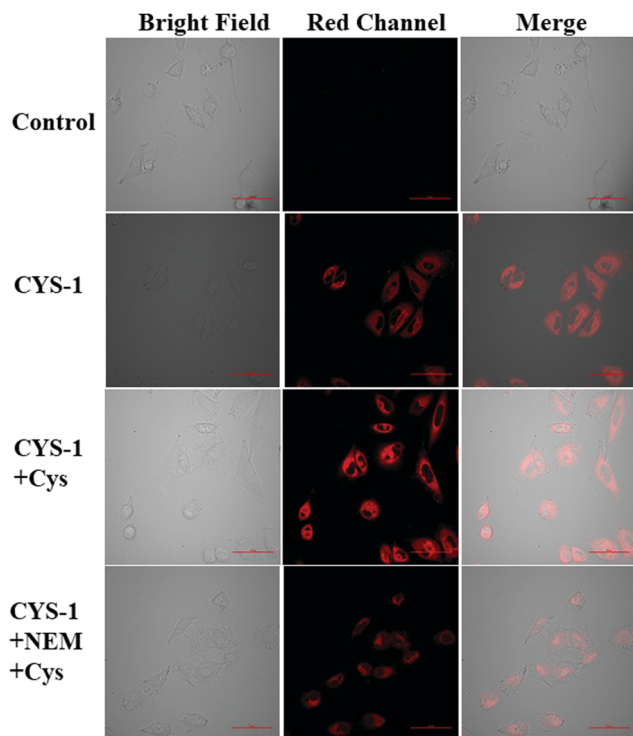


Fig. 7 Fluorescence imaging of cysteine in A549 cells by probe **CYS-1** in cancer cells. Fluorescence images of A549 cells treated without **CYS-1**; fluorescence images of A549 cells treated with **CYS-1** (10  $\mu\text{M}$ ); and fluorescence images of A549 cells treated with **CYS-1** (10  $\mu\text{M}$ ) after being incubated with cysteine (20  $\mu\text{M}$ ). Fluorescence images of A549 cells treated with **CYS-1** (10  $\mu\text{M}$ ) after being incubated with NEM (1 mM) and cysteine (20  $\mu\text{M}$ ). The images were taken under a laser confocal microscope. Scale bar: 50  $\mu\text{m}$ .

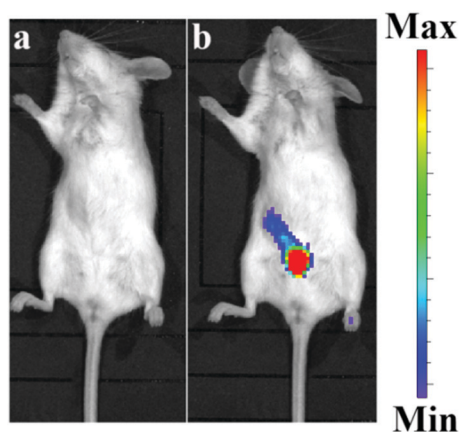


Fig. 8 Fluorescence imaging of cysteine in living mouse. (a) Fluorescence imaging in living mouse after injecting PBS (100  $\mu\text{L}$ ); (b) fluorescence imaging in living mouse after injecting **CYS-1** and cysteine (200  $\mu\text{M}$ , 50  $\mu\text{L}$ ) for 25 min. The images were excited with a 500–600 nm filter, and acquired with a 600–700 nm long-pass filter.

was observed in the second group. Obviously, these data showed that the probe can be used for the imaging of cysteine *in vivo*, indicating that **CYS-1** had great potential in the detection of cysteine *in vivo*.

## Conclusions

In conclusion, this study aimed to modify a dicyanoisophorone-based fluorophore platform with an optically hydroxyl tuneable group for better biocompatibility for molecular bioimaging *in vivo*, chloro-substituted dicyanoisophorone-based **DCM-COH** ( $\lambda_{\text{ex/em}} = 490/655 \text{ nm}$ ) with long emission wavelength and large Stokes shift was constructed and synthesized as a new fluorophore with NIR emission under physiological conditions. In addition, it has excellent chemical and optical properties, such as simple preparation (one-step synthesis), suitable  $\text{pK}_{\text{a}}$  (7.60), a NIR emission for deeper tissue penetration in a physiological environment, and a large Stokes shift (165 nm) which shows a wide range of potential application prospects. As a proof-of-concept, **DCM-COH** has been successfully applied to the design of a probe (**CYS-1**) for detecting cysteine. **CYS-1** possessed a large Stokes shift (165 nm), low toxicity, high sensitivity (detection limit of  $\sim 173 \text{ nM}$ ), good cell membrane permeability, and selectivity for the rapid detection of cysteine. More importantly, the NIR emission fluorescence of the probe had fast response and low background interference, which made it possible to detect cysteine *in vivo*, indicating that the probe could be applied as a promising tool for detecting cysteine in complex bio-systems and diagnosing cysteine-associated diseases in clinical trials. We hope that the platform of this excellent and easy-to-use NIR fluorophore (**DCM-COH**) with an optically tunable hydroxyl group may be exploited for the capable tracking of various analytes in biological chemistry and preclinical applications.

## Conflicts of interest

There are no conflicts to declare.

## Acknowledgements

This research work was supported by the National Natural Science Foundation of China (Grant No. 81903770) and the Joint Construction Project of Medical Science and Technology Research Plan of Henan Province, LHGJ20190266.

## Notes and references

- W. Zhang, F. Liu, C. Zhang, J. G. Luo, J. Luo, W. Yu and L. Kong, *Anal. Chem.*, 2017, **89**, 12319–12326.
- W. Zhang, J. Liu, Y. Yu, Q. Han, T. Cheng, J. Shen, B. Wang and Y. Jiang, *Talanta*, 2018, **185**, 477–482.
- W. Zhang, Y. Wang, J. Dong, Y. Zhang, J. Zhu and J. Gao, *Dyes Pigm.*, 2019, **171**, 107753.
- X. Zhang, C. Liu, X. Cai, B. Tian, H. Zhu, Y. Chen, W. Sheng, P. Jia, Z. Li, Y. Yu, S. Huang and B. Zhu, *Sens. Actuators, B*, 2020, 127820, DOI: 10.1016/j.snb.2020.127820.
- Y. Zhang, Y. Ma, Z. Wang, X. Zhang, X. Chen, S. Hou and H. Wang, *Analyst*, 2020, **145**, 939–945.
- Y. Zhao, K. Wei, F. Kong, X. Gao, K. Xu and B. Tang, *Anal. Chem.*, 2019, **91**, 1368–1374.

- 7 Y. Cai, J. Fang, H. Zhu, W. Qin, Y. Cao, H. Yu, G. Shao, Y. Liu and W. Liu, *Sens. Actuators, B*, 2020, **303**, 127214.
- 8 D. Chen, Z. Long, Y. Dang and L. Chen, *Dyes Pigm.*, 2019, **166**, 266–271.
- 9 J. Ma, T. Si, C. Yan, Y. Li, Q. Li, X. Lu and Y. Guo, *ACS Sens.*, 2020, **5**, 83–92.
- 10 X. Han, X. Song, B. Li, F. Yu and L. Chen, *Biomater. Sci.*, 2018, **6**, 672–682.
- 11 Z. Li, *Talanta*, 2020, 120804, DOI: 10.1016/j.talanta.2020.120804.
- 12 X. Pei, F. Huo, Y. Yue, T. Chen and C. Yin, *Sens. Actuators, B*, 2020, **304**, 127431.
- 13 Y. Yue, F. Huo, P. Yue, X. Meng, J. C. Salamanca, J. O. Escobedo, R. M. Strongin and C. Yin, *Anal. Chem.*, 2018, **90**, 7018–7024.
- 14 H. Zhang, W. Li, J. Chen, G. Li, X. Yue, L. Zhang, X. Song and W. Chen, *Anal. Chim. Acta*, 2020, **1097**, 238–244.
- 15 L. Zhai, Z. Shi, Y. Tu and S. Pu, *Dyes Pigm.*, 2019, **165**, 164–171.
- 16 R. Peng, J. Yuan, D. Cheng, T. Ren, F. Jin, R. Yang, L. Yuan and X. Zhang, *Anal. Chem.*, 2019, **91**, 15974–15981.
- 17 X. Tian, F. Yan, J. Zheng, X. Cui, L. Feng, S. Li, L. Jin, T. D. James and X. Ma, *Anal. Chem.*, 2019, **91**, 15840–15845.
- 18 X. Kong, M. Li, B. Dong, Y. Yin, W. Song and W. Lin, *Anal. Chem.*, 2019, **91**, 15591–15598.
- 19 L. Fang, X.-Y. Zhang, Q. Yuan, D.-D. Li, Q.-C. Jiao, Y.-S. Yang and H.-L. Zhu, *Dyes Pigm.*, 2020, **175**, 108122.
- 20 S. C. Hong, D. P. Murale, S. Y. Jang, M. M. Haque, M. Seo, S. Lee, D. H. Woo, J. Kwon, C. S. Song, Y. K. Kim and J. S. Lee, *Angew. Chem., Int. Ed.*, 2018, **57**, 9716–9721.
- 21 J. Xiong, L. Xia, L. Li, M. Cui, Y. Gu and P. Wang, *Sens. Actuators, B*, 2019, **288**, 127–132.
- 22 Y. Zheng, D. Pan, Y. Zhang, Y. Zhang and Y. Shen, *Anal. Chim. Acta*, 2019, **1090**, 125–132.
- 23 Y. Liu, L. Teng, C. Xu, H.-W. Liu, S. Xu, H. Guo, L. Yuan and X.-B. Zhang, *Chem. Sci.*, 2019, **10**, 10931–10936.
- 24 T. Xue, Y. Dai, X. Zhang, Y. Cheng, X. Gu, H. Ji, S. Misal and Z. Qi, *Sens. Actuators, B*, 2019, **293**, 265–272.
- 25 K. Wang, C.-X. Zhao, T.-H. Leng, C.-Y. Wang, Y.-X. Lu, Y.-J. Shen and W.-H. Zhu, *Dyes Pigm.*, 2018, **151**, 194–201.
- 26 X. Qiu, X. Jiao, C. Liu, D. Zheng, K. Huang, Q. Wang, S. He, L. Zhao and X. Zeng, *Dyes Pigm.*, 2017, **140**, 212–221.
- 27 S. Gong, J. Hong, E. Zhou and G. Feng, *Talanta*, 2019, **201**, 40–45.
- 28 J. Hou, P. Cai, C. Wang and Y. Shen, *Tetrahedron Lett.*, 2018, **59**, 2581–2585.
- 29 J. Li, F. Huo, Z. Wen and C. Yin, *Spectrochim. Acta, Part A*, 2019, **221**, 117156.
- 30 Y. Li, Y. Wang, S. Yang, Y. Zhao, L. Yuan, J. Zheng and R. Yang, *Anal. Chem.*, 2015, **87**, 2495–2503.
- 31 H. Niu, B. Ni, K. Chen, X. Yang, W. Cao, Y. Ye and Y. Zhao, *Talanta*, 2019, **196**, 145–152.
- 32 S. Li, D. Song, W. Huang, Z. Li and Z. Liu, *Anal. Chem.*, 2020, **92**, 2802–2808.
- 33 Q. Hu, C. Yu, X. Xia, F. Zeng and S. Wu, *Biosens. Bioelectron.*, 2016, **81**, 341–348.
- 34 J. Liu, M. Liu, H. Zhang, X. Wei, J. Wang, M. Xian and W. Guo, *Chem. Sci.*, 2019, **10**, 10065–10071.
- 35 Y. Wang, L. Zhang, S. Zhang, Z. Liu and L. Chen, *Anal. Chem.*, 2019, **91**, 7812–7818.
- 36 H. Zhang, C. Yan, H. Li, L. Shi, R. Wang, Z. Guo and W.-H. Zhu, *ACS Appl. Bio Mater.*, 2020, DOI: 10.1021/acsabm.0c00260.
- 37 L. Zhao, X. He, Y. Huang, J. Li, Y. Li, S. Tao, Y. Sun, X. Wang, P. Ma and D. Song, *Sens. Actuators, B*, 2019, **296**, 126571.
- 38 D. Zhu, X. Yan, A. Ren, W. Xie and Z. Duan, *Anal. Chim. Acta*, 2019, **1058**, 136–145.